

Development of 460 GHz and Dual Polarization SIS Mixers for the Submillimeter Array

Chao-Te Li, Kuan-Yu Liu, Wei-Chun Lu, Chuang-Ping Chiu, Tse-Jun Chen, Chong-Wen Chen, Yung-Chin Chang, Ming-Jye Wang, and Sheng-Cai Shi, *Member, IEEE*

Abstract—A heterodyne receiver incorporating superconductor-insulator-superconductor (SIS) mixers has been designed to cover the frequency range from 400 to 520 GHz of the Submillimeter Array (SMA). Various tuning circuits have been employed to resonate out the geometric capacitance of the junction and provide impedance matching to the waveguide probe. Our measurements indicated that a receiver noise temperature of around 90 K, with the contributions from the input noise and intermediate frequency (IF) noise estimated to be around 60 K and 10 K, respectively. SIS mixers integrated with planar orthomode transducers (OMT) have also been designed at 345 GHz for dual polarization detections, and results from the 3-dimensional (3-D) electromagnetic (EM) simulations are presented.

Index Terms—Orthomode transducer, polarization, SIS mixer, submillimeter array.

I. INTRODUCTION

THE Submillimeter Array (SMA), constructed by the Smithsonian Astrophysical Observatory (SAO) and Institute of Astronomy and Astrophysics, Academia Sinica (ASIAA), is a radio interferometer with eight 6-meter antennas. The aim of the array is to explore the submillimeter wavelengths with high angular resolution via interferometric techniques [1]. Fixed tuned receivers equipped with superconductor-insulator-superconductor (SIS) mixers are currently in use for observations through the major submillimeter atmospheric windows from below 200 GHz to above 900 GHz. A total of four receivers that cover the 200, 300, 380, and 660 GHz bands are now in operation. Designs of the 200 and 300 GHz receivers can be found in [2] and [3].

This paper describes the development of the 400–520 GHz SIS mixers and the design of the dual polarization mixer around 345 GHz as options for future upgrades of the SMA. For the 460 GHz SIS mixer, various tuning circuits have been employed in the designs, and comparisons between the test results and simulations are hereby presented. The embedding impedance for optimum receiver performance is also discussed in an effort to come up with a design reference. To increase the speed of

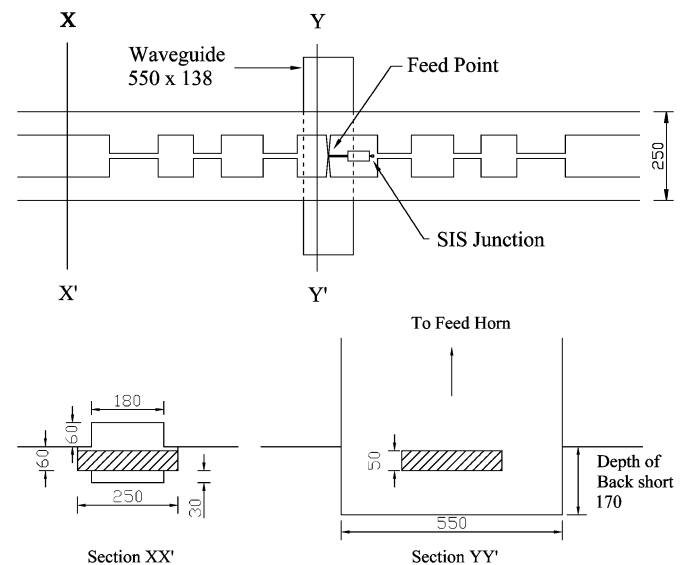


Fig. 1. *Upper*: top view of the reduced height waveguide probe design, illustrating the bowtie probe and the suspended substrate filter layout. *Lower*: sectional view of the mixer block central portion, with the quartz substrate hatched. The cross section of the suspended microstrip and the fixed back-short of the block are shown. All dimensions are in μm .

the array significantly, antennas equipped with multi-pixel receivers are under consideration [4]. Observations with dual polarizations will result in increased sensitivity, and provide further information on the polarization. To realize these concepts, it is essential to develop a compact mixing unit with an integrated orthomode transducer (OMT). In our design, radiations of orthogonal polarizations in the circular waveguide are coupled onto microstrip lines with a planar OMT. Silicon nitride (SiN) membranes, used to support the probes across the waveguide, reduce the perturbations from the substrate and prevent energy leakages out of the substrate channel [5]. Additionally, choke structures and ground rings are utilized to confine the RF within the waveguide and suppress resonances due to the gap within the split block. The results from the 460 GHz mixers were subsequently applied to the tuning circuit design for the dual-polarization mixer.

II. 460 GHz SIS MIXER

A. Waveguide Probe Design

The mixer block utilizes a reduced height waveguide section, along with a bow-tie probe to provide low feed point impedance and wideband performance, as shown in Fig. 1. A fixed back-short, measuring 170 μm in depth, serves to tune the probe impedance. The backshort is configured such that the feed point

Manuscript received August 03, 2010; accepted December 04, 2010. This work was supported by the Institute of Astronomy and Astrophysics, Academia Sinica, Taiwan.

C.-T. Li, K.-Y. Liu, W.-C. Lu, C.-P. Chiu, T.-J. Chen, C.-W. Chen, Y.-C. Chang, and M.-J. Wang are with the Institute of Astronomy and Astrophysics, Academia Sinica, Taipei, 10617, Taiwan (e-mail: ctli@asiaa.sinica.edu.tw).

S.-C. Shi is with the Purple Mountain Observatory, National Astronomical Observatories of China, Nanjing 210008, China (e-mail: scshi@mail.pmo.ac.cn).

Digital Object Identifier 10.1109/TASC.2010.2098835

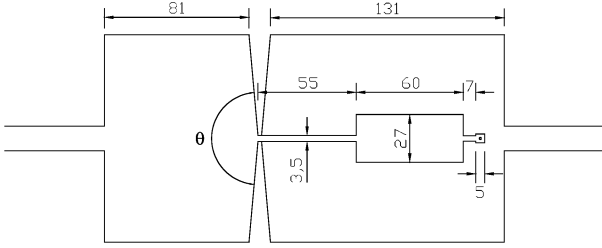


Fig. 2. Layout of the integrated microstrip tuning structure showing the SIS junction, the inductive line and the two step impedance transformer (all dimensions in μm). The tuning circuit runs on top of the RF choke metallization, which serves as a ground plane for thin-film microstrip lines.

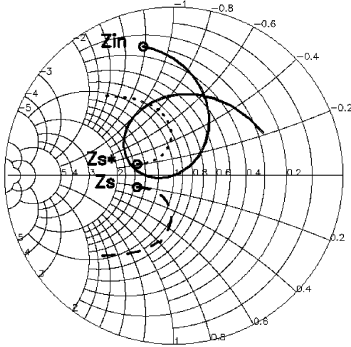


Fig. 3. Simulated feed point impedance of the waveguide probe (dashed line) and its complex conjugate (dotted line) in the 400–520 GHz frequency range. The solid line indicates the input impedance of the design with a series transformer, as shown in Fig. 2. The admittance Smith chart is normalized to $(50 \Omega)^{-1}$. The circles mark the impedance at 400 GHz.

impedance resides in the capacitive region of the Smith chart for stability considerations. For the bow-tie probe, a broad probe (larger θ in Fig. 2) yields a low impedance and effects a better matching with the SIS junction. The length of the probe yields more effect on the imaginary part of the impedance, which becomes more capacitive as one side of the probe is extended to accommodate the tuning circuit. The following RF chokes present an open at RF, thereby cutting down on the transmission of RF signals to the mixer IF port. The embedding impedance of the waveguide probe, simulated with a 3-D EM simulator (HFSS), is shown in Fig. 3.

B. Tuning Circuit

There exist three commonly used tuning schemes in SIS mixer designs for canceling the junction capacitance, namely, the shunt inductance type [6], the end-loaded type [2], and the parallel-connected twin junction (PCTJ) approach [7]. The first one typically results in a relatively high impedance after tuning, compared to the end-loaded approach. One drawback is a rather large capacitance at low frequencies due to an open stub, which limits the IF bandwidth. It is more straightforward to adopt a design with a single junction to suppress the Josephson current, rather than the twin-junction design. In our designs, the end-loaded and the shunt inductance approaches with a single junction have been adopted. The shunt inductance is terminated in a 90° radial stub with a radius of $37 \mu\text{m}$. The radial stub was designed using the classical formulas [8] with the effective

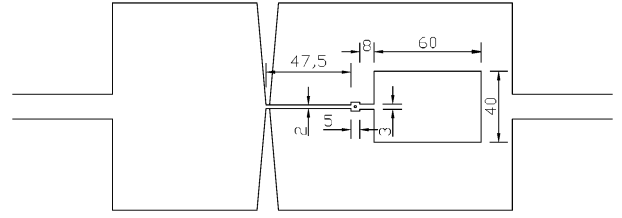


Fig. 4. SIS junction tuned with shunt inductance and a rectangular stub. One transformer is placed between the junction and the feed point for the small impedance difference. All dimensions are in μm .

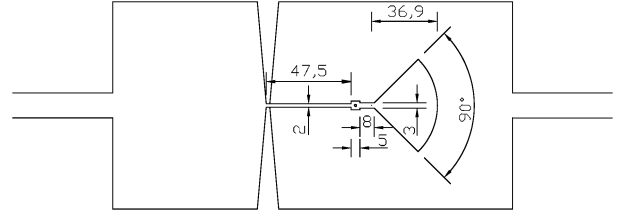


Fig. 5. Tuning circuit and impedance transformer for a SIS junction tuned with shunt inductance. The shunt inductance is terminated in a radial stub. All dimensions are in μm .

magnetic permeability μ_r of the superconducting film taken into account, namely,

$$X_{in} = \frac{h}{\alpha r_1} Z_0(r_1) \frac{\cos(\theta_1 - \phi_2)}{\sin(\phi_1 - \phi_2)}, \quad (1a)$$

$$Z_0(r_1) = \frac{120\pi\sqrt{\mu_r}}{\sqrt{\epsilon_r}} \sqrt{\frac{J_0^2(kr_1) + N_0^2(kr_1)}{J_1^2(kr_1) + N_1^2(kr_1)}} \quad (1b)$$

where α is in radian, and μ_r is close to 1.9 in our case. The radial stub has the same effect as a straight open stub with a characteristic impedance of around 3Ω , close to $Z_0(r_1)$ multiplied by the factor $h(\alpha r_1)^{-1}$. The radial stub can also be synthesized using short strips of various widths. The reactance X_{in} from both methods are comparable, with a similar slope with respect to the frequency and a small offset in the resonant frequency where X_{in} becomes zero. Another version uses a quarter-wavelength low-impedance ($Z_0 = 1.5 \Omega$) rectangular stub. The end-loaded scheme consists of a 3-section series transformer. The first short section of the microstrip line tunes out the junction capacitance and converts the input impedance Z_{in} of the junction to a low resistance $R' = R_n/(\omega R_n C_j)^2$. A two-step transformer is then used to bring Z_{in} up to few tens of Ω . The designs were simulated using the quantum mixer theory [9] and the analytic model for thin-film superconducting microstrip lines [10]. During simulations, the following characteristics of the Nb/Al – AlO_x/Nb tunnel junction are assumed—a normal state resistance R_n of 19.5Ω , current density J_c of 10 kA/cm^2 , junction area of $1 \mu\text{m}^2$, and junction capacitance of 90 fF . Nb/SiO₂/Nb microstrip lines with a 2500 \AA thick insulating layer are used for the tuning circuits. The final designs with the three different tuning circuits are shown in Figs. 2, 4, and 5.

C. Embedding Impedance for Optimum Receiver Performance

To investigate the optimum embedding impedance for better receiver performance, we have adopted a design with shunt in-

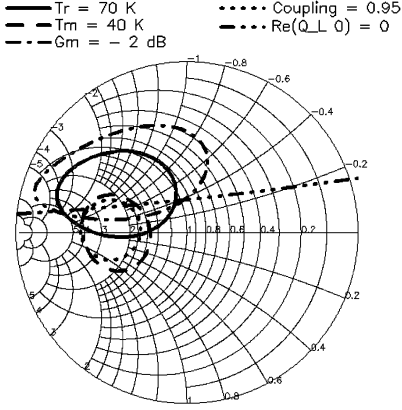


Fig. 6. Contour of T_R (full line) enclosing the region where T_R is less than 70 K. Similarly, regions for T_M less than 40 K (dashed), G_M better than -2 dB (dot-dash), and coupling better than 95% (dotted) are enclosed by the corresponding contours on the Smith chart for the design with shunt inductance and a rectangular stub at 485 GHz. The dash-dot-dot-dot line marks where the $\text{Re}(Q_L^0) = 0$. $\text{Re}(Q_L^0) < 0$ in the upper region.

ductance, in which the input impedance of the SIS junction is not transformed to a small value by series inductance, as is the case with the end-loaded scheme. At the LO of 485 GHz, where the junction capacitance is cancelled in our design, the receiver noise temperature T_R , mixer noise temperature T_M , mixer conversion gain G_M , coupling, and the mixer output conductance G_L^0 [11] were simulated with respect to different embedding impedances on the Smith chart. Here

$$T_R = T_M + \frac{T_{IF}}{G_M}. \quad (2)$$

In Fig. 6, the contours of T_R , T_M , G_M , coupling, and $\text{Re}(G_L^0)$, the real part of G_L^0 , are plotted. It shows that the minimum T_R can be achieved over a rather broad range on the Smith chart, close to where G_M is optimized. However, the T_M contour does not coincide with its T_R counterpart, and is instead aligned with the coupling. In term of the stability and gain linearity [12], it is preferred to operate the SIS junction without any significant conversion gain. Therefore, the region enclosed by the T_M contour is likely a better choice for optimum receiver performance. The contour is centered around a source conductance of 2.5 (normalized to $(50 \Omega)^{-1}$), consistent with the optimum source conductance derived from the empirical formula in [13]

$$G_s = \frac{1}{2} + \frac{1}{4\omega}. \quad (3)$$

D. Receiver Performance

The receiver performance has been measured with different SIS junctions and tuning circuits over an LO frequency range from 380 GHz to 540 GHz. The double-sideband (DSB) receiver noise temperature was determined by the Y-factor method using hot and cold loads as the broadband signal sources. The shot noise produced by the resistance in the linear portion of the junction I-V curve for voltages higher than the gap voltage was used to calibrate the IF system noise and gain, thereby allowing for the estimation of the mixer conversion gain. The input noise from the optical loss T_{in} can be estimated

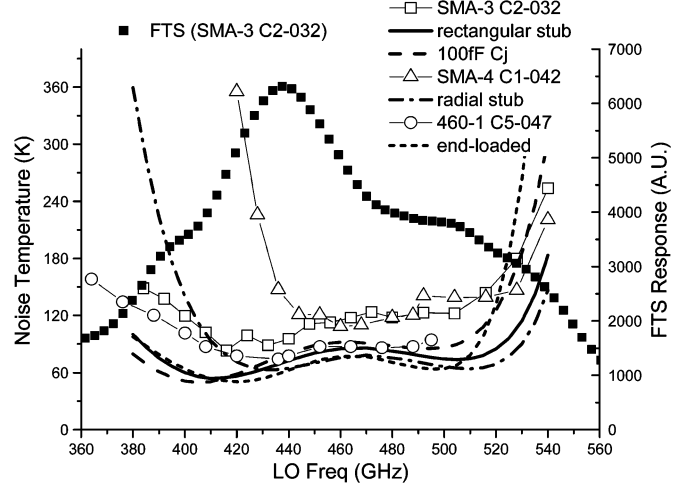


Fig. 7. Receiver noise temperature T_R as a function of LO frequency for three SIS mixers with different tuning circuits. The squares denote the measured double-sideband (DSB) T_R for a device using a parallel tuning circuit with a quarter-wavelength stub. The solid line represents the simulated single sideband (SSB) T_R of the design, and the dash line the simulations with a larger C_j . The FTS responses are displayed as closed squares. The 2nd device (triangles) has a parallel inductance with a radial stub, while the dash-dot line represents the simulation result. The 3rd device (circles) utilizes a series transformer, and the simulations are shown as the dotted line.

using the intersecting-line method [14]. Measurements of devices with the end-loaded design were in good agreement with simulations [15]. For the design with shunt inductance and a radial stub, the measurement results exhibited a similar frequency response to the simulations, albeit with a smaller bandwidth. From measurements of a junction with a rectangular open stub, the best performance occurred at 416 GHz, which yielded $T_R = 83$ K (Y-factor = 2.48) and a positive conversion gain of 1.6 dB (including the loss of RF path). The negative slope of the pumped dc I-V characteristic [16] appeared at frequencies below 420 GHz, consistent with the simulations. The receiver exhibited a receiver noise temperature of 90–120 K in the frequency range from 400 to 500 GHz after correcting for the loss through the LO wire grid as shown in Fig. 7. The increase in noise at higher frequencies, which was inconsistent with the simulations, could be accounted for by an increase in the junction capacitance C_j . The simulation with C_j of 100 fF is also shown as the dashed curve in Fig. 7. The T_{in} was estimated to be 60–80 K and the noise from the IF system T_{IF} to be around 10 K. To investigate the response of the receiver over a wider frequency range, the device was measured with a Fourier transform spectrometer (FTS). The FTS response tracks the receiver noise as both the T_M and FTS response are closely related to the coupling.

III. DUAL POLARIZATION SIS MIXER

An orthomode transducer (OMT) is critical for separating the two polarizations of the incoming radiation. While planar OMTs have previously been integrated with transition-edge sensors (TES) in polarimeters [17], [18], our planar OMT consists of two rectangular probes suspended on a 1–2 μm silicon nitride membrane inside a circular waveguide. The waveguide is terminated in a back-short approximately one quarter wavelength behind the probe. Each probe couples radiation of orthogonal

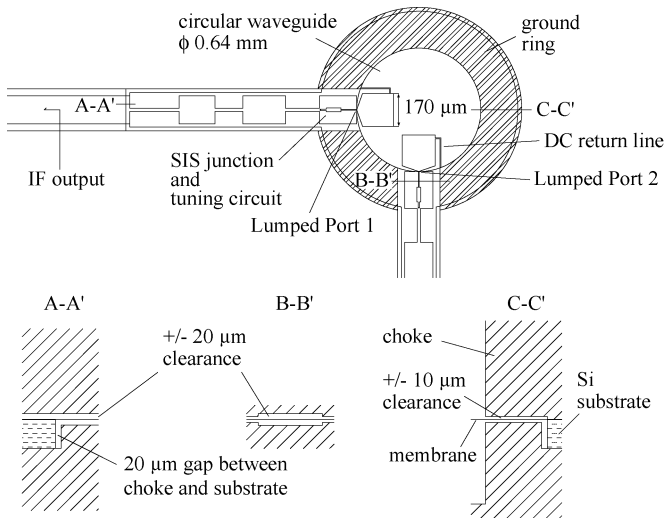


Fig. 8. The top view of the 2-probe OMT in a circular waveguide. Rectangular probes are implemented on a $1\text{--}2\ \mu\text{m}$ thick suspended membrane. SIS junctions with series tuning circuits are also shown. Sectional views show the cross section of the membrane, the silicon substrate, and the choke structure at 3 different places of the design.

TE_{11} modes from the circular waveguide onto microstrip transmission lines. The circular waveguide of 0.64 mm in diameter has a TE_{11} mode cut-off frequency of around 275 GHz.

One unit of a large-format detector array with the substrate extending to the edges of the split block was simulated. One challenge for this structure is to confine the RF signal within the circular waveguide to avoid resonances. Several approaches have been adopted as described below. The membrane structure, used to support the probes and the RF chokes, makes possible a reduction in the opening in the waveguide wall, and increases the cut-off frequency of the waveguide modes along the IF channel above the RF band. A $100\ \mu\text{m}$ thick Si substrate is present outside these regions as the support base. A ground ring, quarter wavelength in radius, presents a short to the waveguide, and six-section RF chokes provide a RF ground to the lumped port following the probe. Choke structures are used on both the top and bottom mixer blocks to fill the gap around the waveguide. There are $10\ \mu\text{m}$ gaps above and below the membrane with metal boundaries defined by the choke structure. The purpose of the $20\ \mu\text{m}$ gap is to accommodate machining tolerances in the split block and possible wrinkling in the silicon nitride membrane, as shown in Fig. 8.

The probe design was optimized with a 3-D EM simulator (HFSS) to obtain the feed point impedance converging around $50\ \Omega$. Although the optimum source resistance is also around $20\ \Omega$ with a R_n of $19.5\ \Omega$, the waveguide probe would have become too wide to reach that impedance level. From our simulations, the co-polarization coupling was over 90% and the cross polarization was less than $-20\ \text{dB}$ with respect to a lumped port of $50\ \Omega$ over 310–370 GHz, as shown in Fig. 9. A high impedance line between the probe and the ground ring serves as the DC bias return. For the tuning circuit, we adopt the end-loaded design as it exhibits a comparable or larger bandwidth from the testing of the 460 GHz mixers.

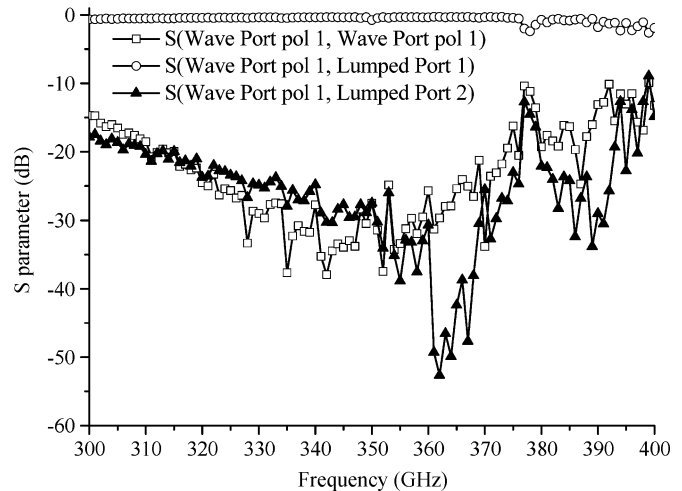


Fig. 9. Simulated S-parameters for the 2-probe OMT in the 300–400 GHz frequency range. The circles give the co-polarization power coupling for one linear polarization. The squares show the power reflection out of the input waveguide and the triangles give the cross polarization coupling. To get a realistic sense of the loss, all metals, except for the waveguide, have been assigned the conductivity of copper ($5.8 \times 10^7\ \text{S/meter}$).

IV. CONCLUSION

SIS junction mixers with two tuning schemes were developed for the SMA 400–520 GHz band. Measurements of devices with end-loaded tuning circuits were more consistent with simulations. From our simulations, the embedding impedance for optimum receiver performance was determined to be where the coupling is efficient on the Smith chart. A large-format detector array with dual polarization capability is under consideration as an option for SMA upgrade. One element equipped with a planar OMT and SIS junction mixers was simulated at around 350 GHz, and over 90% co-polarization coupling and convergent feed point impedance have been achieved.

ACKNOWLEDGMENT

The authors thank C. E. Tong for the 460 GHz band mixer block design and fruitful discussions.

REFERENCES

- [1] P. T. P. Ho, J. M. Moran, and K. Y. Lo, "The submillimeter array," *The Astrophysical Journal*, vol. 616, pp. L1–L6, Nov. 2004.
- [2] R. Blundell, C. Y. E. Tong, D. C. Papa, R. L. Leombruno, X. Zhang, S. Paine, J. A. Stern, H. G. LeDuc, and B. Bumble, "A wideband fixed-tuned SIS receiver for 200-GHz operation," *IEEE Trans. Microwave Theory and Techniques*, vol. 43, pp. 933–937, 1995.
- [3] C. E. Tong, R. Blundell, S. Paine, D. C. Papa, J. Kawamura, X. Zhang, J. A. Stern, and H. G. LeDuc, "Design and characterization of a 250–350 GHz fixed-tuned superconductor-insulator-superconductor receiver," *IEEE Trans. Microwave Theory and Techniques*, vol. 44, pp. 1548–1556, 1996.
- [4] A. R. Gillespie and T. G. Phillips, "Array detectors for millimetre line astronomy," *A&A*, vol. 73, pp. 14–18, 1979.
- [5] J. W. Kooi, G. Chattopadhyay, S. Withington, F. Rice, J. Zmuidzinas, C. Walker, and G. Yassin, "A full-height waveguide to thin-film microstrip transition with exceptional RF bandwidth and coupling efficiency," *Int. J. IR and MM Waves*, vol. 24, no. 3, pp. 261–284, 2003.
- [6] A. R. Kerr, S. K. Pan, and M. J. Feldman, "Integrated tuning elements for SIS mixers," *Int. J. Infrared & Mm Waves*, vol. 9, no. 2, pp. 203–212, 1988.

- [7] S. C. Shi, T. Noguchi, and J. Inatani, "A new type of SIS mixer using parallel-connected twin junctions," in *Conf. Dig. 19th Int. Conf. on IR and MM Waves*, Sendai, Japan, 1994, pp. 110–111.
- [8] H. A. Atwater, "Microstrip reactive circuit elements," *Microwave Theory and Techniques*, vol. MTT-31, pp. 488–491, 1983.
- [9] J. R. Tucker, "Quantum limited detection in tunnel junction mixers," *IEEE Journal of Quantum Electronics*, vol. QE-15, pp. 1234–1258, 1979.
- [10] W. H. Chang, "The inductance of a superconducting strip transmission line," *J. Appl. Phys.*, vol. 50, pp. 8129–8134, 1979.
- [11] J. R. Tucker and M. J. Feldman, "Quantum detection at millimeter wavelengths," *Reviews of Modern Physics*, vol. 57, pp. 1055–1113, 1985.
- [12] A. R. Kerr, "Saturation by noise and CW signals in SIS mixers," in *Proc. 13th Int. Symp. on Space Terahertz Technology*, March 2002.
- [13] Q. Ke and M. J. Feldman, "Optimum source conductance for high frequency superconducting quasiparticle receivers," *IEEE Trans. Microwave Theory Tech.*, vol. 41, pp. 600–604, 1993.
- [14] R. Blundell, R. E. Miller, and K. H. Gundlach, "Understanding noise in SIS receivers," *Int. J. IR and MM Waves*, vol. 13, no. 1, pp. 3–26, 1992.
- [15] C. T. Li, T. J. Chen, T. L. Ni, and W. C. Lu *et al.*, "Development of SIS mixers for SMA 400–520 GHz band," in *Proc. 20th Int. Symp. on Space Terahertz Technology*, April 2009.
- [16] W. Shan, Z. Li, J. Zhong, and S. C. Shi, "An 85–115 GHz SIS mixer demonstrating nearly constant dynamic resistance," *IEEE Trans. Applied Superconductivity*, vol. 19, pp. 432–435, 2009.
- [17] J. McMahon, J. W. Appel, and J. E. Austerlmann *et al.*, "Planar orthomode transducers for feedhorn-coupled TES polarimeters," in *Proc. 13th Int. Workshop on Low Temperature Detectors*, Stanford, 2009, pp. 490–493.
- [18] P. Mauskopf, P. Ade, S. Withington, J. Zhang, and P. Grime, "Clover polarimetric detector—A novel design of an orthomode transducer at 150 and 225 GHz," in *Proc. Progress in Electromagnetics Research Symp.*, Hangzhou, China, 2008, pp. 173–176.